Sigma J Eng & Nat Sci 38 (1), 2020, 29-46

Sigma Journal of Engineering and Natural Sciences
Sigma Mühendislik ve Fen Bilimleri Dergisi

Research Article

SEPARATION OF Co(II) AND Se(VI) FROM A METAL AND GLASS INDUSTRY WASTES USING GRAPHENE OXIDE-MANGANE OXIDE NANOCOMPOSITE

Sevil AKÇAĞLAR*[1]

[1]*Dokuz Eylül University, Dept. of Mechanical Engineering, Buca-İZMIR;* ORCID: 0000-0002-5386-1862

Received: 19.02.2019 Revised: 17.06.2019 Accepted: 01.11.2019

ABSTRACT

Co(II) and Se(VI) were not removed with conventional biological treatments, adsorption and chemical processes. Graphene oxide and mangane are excellent adsorbent for heavy metal remediation since their negative surface charge at an alkaline pH. Therefore, in this study, by doping the mangane oxide to the the graphene oxide Co(II) and Se(VI) were removed. XRD pattern of graphene oxide-mangane oxide samples showed that this nanocomposite exhibits poor cristallinity and contained MnO in Birnessite form. EDS analysis results showed that the graphene oxide has the lowest surface area (32 m^2/g) and pore volume (0.11 cm^3/g) with an average pore size of 17.3 nm. As the pH was increased from 2,0 to 9,0; the negativity of the zeta potantial of graphene oxide- mangane oxide nanocomposite decreased. Tthe narrow O 1s XPS spectra of mangane oxide-graphene oxide nanocomposite contained MnO_2.The FTIR spectra of the nanocomposite showed that hydroxyl and carboxyl groups were present. For maximum Se(VI) and Co(II) adsorptions (98% and 98%); the optimum graphene oxide–mangane oxide concentration was found as 4 mg/L, at a pH of 8.9 at 21 ^{0}C after 20 min contacting time. The adsorption of Co(II) and Se(VI) was explained by the pseudo-first order kinetic model while the maximum adsorption capacities of Co(II) and Se(VI) were 256 mg/g and 289 mg/g, respectively. Graphene oxide–mangane oxide nanocomposite was reused with the percentages of 86% and 90% for Co(II) and Se(VI), respectively after four sequential utilisation. This, reduce the treatment cost by 48% for Se(VI) and by 43% for Co(II).

Keywords: Co(II), Se(VI), metal industry, glass industry, graphene oxide-mangane oxide nanocomposite**,** wastewater, adsorption, reuse, cost.

1. INTRODUCTION

Se is found as selenate (SeO_4^{2-}) and selenite (SeO_3^{2-}) in the oil refinery and glass production wastewaters [1] Cobalt, although is used in the some pharmaceuticals has can be toxic to the health. The natural sources of cobalt in the ecocystem are settled sludge, river and lakes. Cobalt is used in pharmaceutical industry, in the production of nano metal oxides, in electricity and glass industries. The limits of cobalt in the tap water are very low (between 0.05 and 1.0 $mg/dm^{3)}$ [1]

Adsorption studies were performed to detect the removal of selenium in different chemicals, e.g. aluminium oxide [2], manganese nodules [3], [4], activated carbon [5], [6] and magnetite [7]. During adsorption, with efficient and specific adsorbents it is important to recovery the

* Corresponding Author: e-mail: sevil.akcaglar@deu.edu.tr, tel: (532) 617 70 63

adsorbents with simultanoues removal. Nano metal oxides (Mo(IV), Fe(III), Hf(VI), Se(IV) oxides) are used in the treatment of some metals [8], [9]. Big surface area and por sizes are the major requirements for nanocomposites [10], sorption, environmental treatment [11], energy storage devices [12], and water repellant coatings [13].

Metal oxide nanoparticles (NPs) with large porous properties as support material (zeolite, brick and activated carbon) were used as adsorbents [14], [15], [16]. However, sometimes the aggregation of the NPs within the support materials ending with blockage in micropores or mesopores, and this decrease the yield of adsorption efficiency [17]. Zhang et al. suggested a mechanism to reduce the accumulation of adsorbents by doping metal oxide NPs onto aluminated sands [18]. The binding groups elevated the distribution of the metal nanocomposites, and this reduced the absorption of metal oxides. The nanoparticles with big size porosities and loaded groups are important in the production of composite materials.

Graphene oxide has a high density and contains oxygenated groups such as carboxylic and hydroxylic [19], [20], [21]. Under these conditions, the NPs accumulation and the blocking of pores were decreased. This makes graphene oxide an effective support material among NPs. Furthermore, graphene oxide decrease the the resistance during diffusion of the pollutants from the hollows and has a distinguished feature during aggregation of composites at alkaline pH (pH=10). As a result loading of the graphene oxide nanomaterials produces an electrostatic resistance between negatively charged oxygenated groups and pollutants [22]. This improves the conductivity of graphene oxide in the liquid wastes. At high pHs levels (9.0 -10.0) the graphene oxide can be successfully produced. Mangane oxide with a pH_{pzc} of 3 is accepted as a powerfull nanometal for some metal remediation since its surface charge is negative at alkaline pH levels and therefore can be doped to the metals [23].

In this study, a graphene oxide-mangane oxide nanocomposite was produced under laboratory conditions with an alkalinity of 8%. Co(II) and Se(VI) were chosen as the representative metals and the feasibility of adsorbing of Selenium(VI) and Cobalt(II) from glass and metal industry wastewaters was investigated for the first time. The physicochemical properties of graphene oxide-mangane oxide composite were investigated by scanning electron microspcope (SEM), and Nitrogen adsorption/desorption isotherms. X-ray photoelectron spectroscopy (XPS) and scanning TEM-Scanning transmission electron microscopy (STEM) analysis were performed. The surface morphology of the graphene oxide-mangane oxide was performed by high-resolution transmission electron microscopy (HR-TEM). The crystallinity of the graphene oxide-mangane oxide was investigated by X-ray diffraction (XRD). The thermal stability of the graphene oxide-mangane oxide was examined by thermogravimetric analyses (TGA). The zeta potential of graphene oxide-mangane oxide was measured. Furthermore, Scanning electron microscope (SEM), Fourier transform infrared spectroscopy (FT-IR), energy-dispersive X-ray spectroscopy (EDS), and IR Raman spectra analysis were performed. The zeta potential of graphene oxide-mangane oxide and the surface area (*S*BET) was calculated. The effects of increasing graphene oxide-mangane oxide concentrations (1, 2, 3, 4, 5, 6 and 7 mg/L), of contact time (20, 30, 50, 60, 70 and 80 min) and of pHs (2.2, 4.5, 6.2, 8.9 and 10.0) on the adsorption capacities of Se(VI) and Co(II) were investigated. Two adsorption kinetic models (first, second pseudo) were used to detect the removal kinetics of Se(VI) and Co(II). Furthermore, the recoveries of the studied metals were performed after adsorption. A cost analysis was performed for the adsorption processes.

2. MATERIAL AND METH ODS

2.1. Preparation of Nanocomposites

2.1.1. Synthesis of Graphene Oxide-Mangane Oxide nanocomposite

Graphene oxide-mangane oxide was produced from graphite powder using the method proposed by Hummers [24]. 2 g of graphite was put to 100 mL of H_2SO_4 in an box containing ice. 7.0 g of $KMnO_4$ was put to the mixture and stirred for 4 h at 37 °C. Deionized water was spreyed slowly to the luquid which its temperature is 90 °C. Then, 35 mL of 6% H_2O_2 was added to the mixture; and the liquid was filtered with a 0.05 μm pore diameter Millipore membrane. This mixture was washed with 15% HCl and distilled water. Graphene oxide was obtained by using a sonicator. The solid phase was filtered and washed with distilled water. The solid phase was graphene oxide. It was dried and mixed in the deonized water at a concentration of 15 mg/L $KMnO_4$ and is put to the graphen oxide at a volume ratio of 0.05%. This is defined as graphene oxide-mangane oxide nanocomposite. This mixture was put to the sonicator at a power of 89 W cm^{-1} for 30 min. Then, the mixture was filtered and washed with distilled water and methanol. The produced product is graphene oxide-mangane oxide nanocomposite.

2.1.2. Batch Adsorption Studies

Adsorption experiments were performed in 150 mL glass flasks. 0.01 g graphen oxide-mangane oxide was put into 40 mL Se(VI) or Co(II) containing wastewater. The pH was adjusted to 8.5 using 0.1 M NaOH. The flasks were shaken at 278 K at 250 rpm for 22 hours using a shaker. For adsorption kinetics; 0.1*g* graphene oxide-mangane oxide was shaken into 500 mL industry wastewater containing Se (VI) or Co(II) to determine the adsorption kinetics.

2.1.3. Physicochemical Analysis of Graphene Oxide-Mangane Oxide Nanocomposite

The specific surface area and pore size distribution of the graphene oxide, mangane oxide and graphene oxide-mangane oxide nanocomposite were done using a BET surface area analyzer (ASAP2020, USA) by the N_2 adsorption–desorption tests at 89 K. The surface properties of graphene oxide-mangane oxide was detected by a scanning electron microscope (SEM, S-3400 N, Japan) and a high-resolution transmission electron microscopy (HR-TEM, Tecnai G2 F30 S-Twin, USA) containing a field distribution apparatus at 197 kV. Scanning transmission electron microscopy (STEM) analysis was conducted to obtain the distribution of some metals into graphene oxide-mangane oxide. To analyze the organic and inorganic characteristics of the graphene oxide-mangane oxide; Fourier transform infrared spectroscopy (FT-IR) (Nicolet Model 810 FT-IR instrument-Nicolet analytical Instruments, WI) device was used. The crystallinity of the graphene oxide-mangane oxide was investigated by X-ray diffraction (XRD) with Kα radiation and scan rate of 0.04° s^{-1} PRO, USA). The IR Raman spectra of the samples were detected by Horiba JobinYvon, France at λ=532 nm laser power 1.7 mW, 100 x objective lens, 0.9 NA. The energy-dispersive X-ray spectroscopy (EDS) analysis was carried out on Bruker EDS QUANTAX. The thermal stability of the graphene oxide-mangane oxide was examined by thermogravimetric experiments (TGA) (Perkin–Elmer Diamond TG analyzer). Zetasizer Nano ZS 90 was used to measure the zeta potential of graphene oxide-mangane oxide. X-ray photoelectron spectroscopy (XPS, Kratos AXIS Ultra DLD, and Germany) was used to detect the situation of the adsorbed material onto graphene oxide-mangane oxide. The high-resolution Cu $2p_{3/2}$ peak was fitted by a curve-fitting program (XPS-peak4.1). The surface area (*S*BET) was calculated by usng the Brunauer–Emmett–Teller (BET) equation. The total hollow volume (*V*p) was detected at *P*/*P*0 = 0.98 and the adsorption mean hollow size (4 V/A) was determined by BET. Micropore volume

(*V* micro) and the external area (*S*external) were calculated by the *t*-method using an suitable standard.

2.2. Analytical Procedure

2.2.1. Se(VI) Measurement Method

1 mL of glass industry and metal industry wastewater samples was separately digested with 5 mL HNO_3 and H_2O_2 at an oven at 250°C for 20 min and at 250°C for 15 min. After cooling the samples were diluted with 1% HNO_3 and analyzed by ICP-MS. The limit of detection for Se(VI) was $0.39x10^{-2}$ mg/L.

2.2.2. Co (II) Measurement Method

An atomic absorption spectrometer (PG-990, USA) with deuterium and cobalt hollow cathode lamps was utilized for detect the cobalt at a wavelength of 251 nm. The pH of 100mL samples having Co(II) at levels varying between 0.01 and 10 mg/L was adjusted to 2.00 using $3.0x10^{-2}$ mol/L HCl. Then the samples were centrifuged and 0.9 mL of 2-2-Methylimidazole and 0,8 mL Tetrafluoroborate was added into the supernatants. They were stirred and then, 6.0 mL of hexafluoride containing 0.01 g sulfur, and 0.5 mol/L sodium hexafluorophosphate was added. The samples were centrifuged for 20 min at 3800 rpm to separate the solid and liquid phases [25].

2.3. Co(II) and Se(VI) Concentrations in the Glass and Raw Metal Industries

The Co(II) and Se(VI) concentrations concentrations in the raw metal concentrations were about 2.5 mg/L.

2.4. Statistical Analysis

Regression analysis is used to understand the independent variables are related to the dependent variable. Alpha (α) level is the significance of the Analysis of Variance (ANOVA) statistic. In the study α was accepted as 0.05. F value of the analysis was performed using MS Office 2010 Excell program.

3. RESULTS AND DISCUSSION

3.1. Characterization of Graphene Oxide-Mangane Oxide Nanocomposite with SEM

Fig. 1 shows the micro-morphology of 5 mg/L graphene oxide-mangane oxide nanocomposite. Graphene oxide-mangane oxide exhibited a lamellar and a wrinkled morphology. The MnO was doped to the graphene oxide surrounding. A structure with a smooth surface was detected in graphene oxide. A deposition of MnO was detected in the upper layer of the graphene oxide-mangane oxide nanocomposite since the surface of the graphene oxide-mangane oxide is smooth.

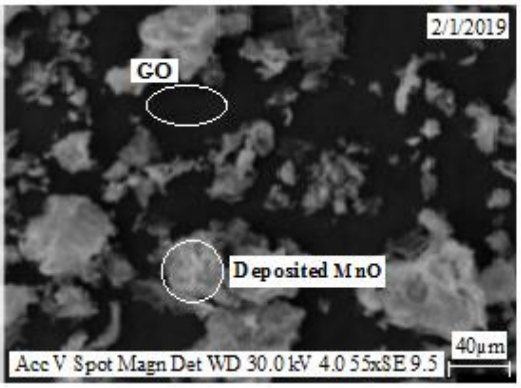

Figure 1. SEM image of 5 mg/L graphene oxide-mangane oxide

3.2. FT-IR Spectra and IR Raman Spectra of Graphene Oxide-Mangane Oxide

The FT-IR spectra of graphene oxide-mangane oxide are given in Fig. 2a. Hydroxylic, carboxylic, and carbonylic groups were detected in the surface of graphene oxide-mangane oxide nanocomposite. The maximum peak observed at around 3250 cm^{-1}. This verify the hydroxylic groups in graphene oxide The C–C peak was detected at 1600 cm^{-1}. A C-O-C peak was detected at 1200 cm^{-1} bonding to carbonylic/carboxylic double C═O with C–O in 1250 cm^{-1} and 1700 cm^{-1}. The detection of an absorption peak at 501 cm^{-1} describe the Mn-O vibration and showed that MnO was bounded to the surface of graphene oxide [26].

The IR–Raman spectra of graphene oxide and graphene oxide-mangane oxide are illustrated in Fig. 2b. The IR spectrum of graphene oxide showed characteristic peaks at 250, 400, 607, 1300 and 1700 cm^{-1}. In the compairison of the two peak bands at graphene oxide and graphene oxide-mangane oxide; the band spectrum of graphene oxide-mangane oxide is lower, showing the formation of the chemical bonds between graphene oxide and MnO.

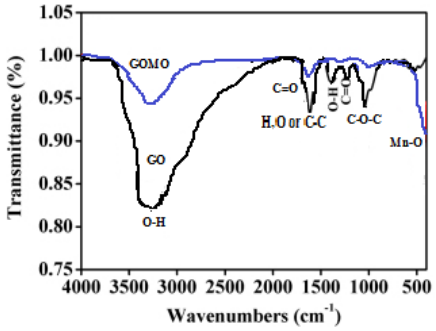

Figure 2a. FTIR spectra of Graphene Oxide-mangane Oxide (GO-MO) and MnO

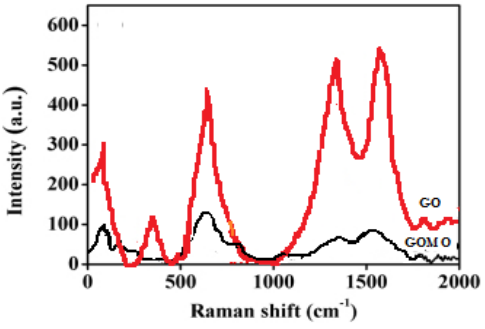

Figure 2b. IR Raman spectra of Graphene Oxide-mangane Oxide (GO-MO) and MnO

Figure 2. The FTIR spectra (**a**) and Raman spectra (**b**) of graphene oxide and graphene oxide-mangane oxide nanocomposte (GO-MO)

3.3. XRD Characterisation of Graphene Oxide-Mangane Oxide

Fig. 3 showed the XRD spectra of graphene oxide-mangane oxide. Graphene oxide-mangane oxide spectra illustrated that the intensity of graphene oxide peaks decreased. The XRD spectra of graphene oxide-mangane oxide samples showed the maximum specific peaks at 2θ = 12,2°, 18,5°, 37,11° and 65° and indicates the existance MnO at a Birnessite type. This shows the presence of MnO on graphene oxide-mangane oxide. All peaks have low intensity, showing the presence of very small crystallized particles. In the position at 2 θ ~ 12-13° and 36-38°, there are two obvious hint of graphene oxide peak (Fig. 3). They were poorly crystallized in the surface of graphene oxide-mangane oxide.

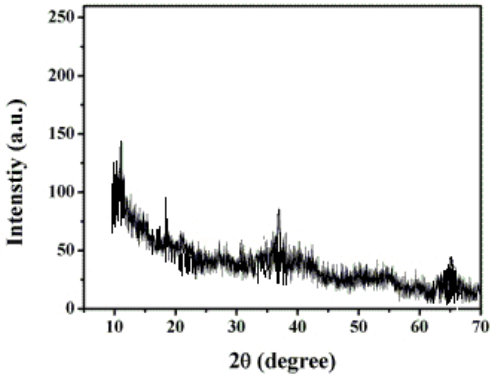

Figure 3. XRD patterns of graphene oxide-mangane oxide

3.4. EDS Analysis

EDS analysis results showed that Mn mass ratio was detected as 17.40 Wt % in graphene oxide-mangane oxide while no pure Mn element was detected in graphene oxide. This showed that the combination is between graphene oxide and MnO **(**data not shown). Furthermore, the graphene oxide-mangane oxide sample contains oxygenophilic functinonal groups (data not shown). This result confirmed that MnO has been coated on the graphene oxide sheets. The results of the surface area and pore structure of graphene oxide is given in Table 1. Graphene oxide has the smallest surface area (32 m^2/g) and pore volume (0.11 cm^3/g), as reported by Li et al., (2013) [27]. The average pore width of graphene oxide is 17.3 nm.This showed that graphene oxide is a mesoporous material. The mesoporous morphology of graphene oxide and its small surface area can be explained by the accumulation of graphene oxide during drying process at 100 ^0C. This can be explained by the van der Waals force between graphene oxide metal oxides.

Table 1. Properties of graphene oxide sample: surface area (S_{BET}), total pore volume (Vp), the average pore width (L)

Sample	$S_{BET}(m^2/g)$	$V_p(cm^3/g)$	L(nm)
Graphene Oxide	32	0.11	17.3

3.5. Zeta Potential of the Graphene Oxide-Mangane Oxide Nanocomposite

The variation of the zeta potentials of graphene oxide, mangane oxide and graphene oxide-mangane oxide nanocomposite versus pH is illustrated in Fig. 4. The aforementioned nano-metal

oxides and graphene oxide- mangane oxide nanocomposite have enlarged their negative zeta potentials (≤15.8 mV) in the pH values varying between 2 and 9. This showed that the particles did not aggregate and were dispersed homogeneously in the wastewater. The negative zeta potential shows that the acidity of nanocomposite surface containing oxygenated functional groups as reported by Amir et al., (2017) [28].

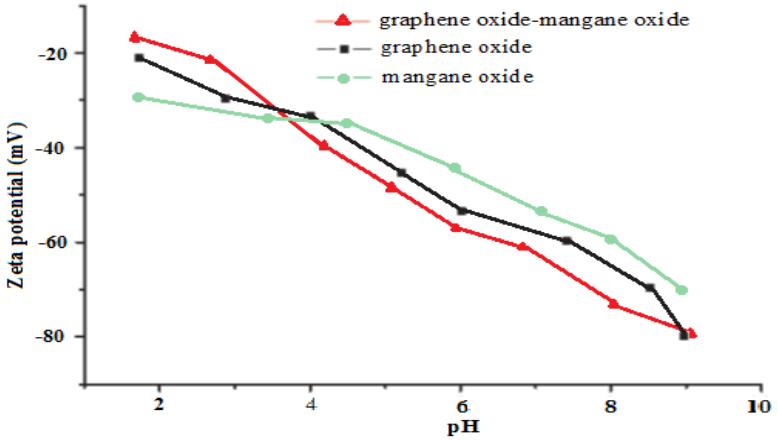

Figure 4. Zeta potential variations versus pH of graphene oxide, mangane oxide and graphene oxide-mangane oxide nanocomposite

3.6. HR-TEM Images of Graphene Oxide, Mangane Oxide and Graphene Oxide-Mangane Oxide Nanocomposite

The HR-TEM image of graphene oxide-mangane oxide nanocomposite is illustrated Fig. 5. In this figure it was observed that the mangane oxide was well dispersed on the graphene oxide. It was showed that the particle size of mangane oxide was 6 nm. With doping of the graphene oxide; the graphene oxide-mangane oxide nanocomposite exhibited crystal morphology and the calculated lattice void was 0.188 nm. This occurred with the distribution of mangane oxide nanoparticles resulted in big BET surface area of graphene oxide-mangane oxide nanocomposite (356.33 m^2/g), which is an order magnitude higher than that of graphene oxide (32 m^2/g) and dispersed mangane oxide (30.98 m^2/g). The BET properties of the graphene oxide and graphene oxide-mangane oxide nanocomposite are summarized in Table 2. The results agree with the findings of Jasinski et al., (2013) [29].

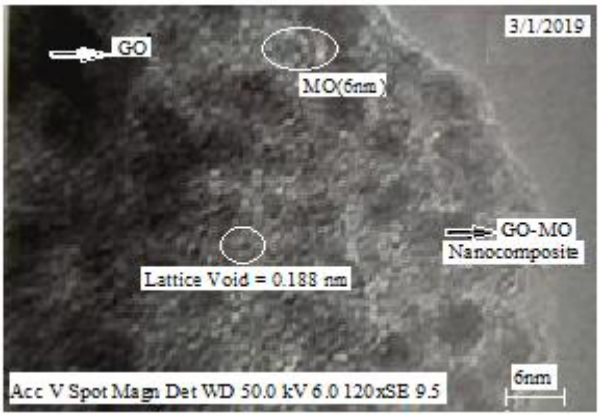

Figure 5. HR-TEM images of graphene oxide, mangane oxide and graphene oxide-mangane oxide nanocomposite

Table 2. BET surface area of graphene oxide, mangane oxide and graphene oxide-mangane oxide nanocomposite

BET surface area (m^2/g)		
graphene oxide	mangane oxide	graphene oxide-mangane oxide nanocomposite
32	30,98	356.33

3.7. XPS Analysis of Graphene Oxide, Mangane Oxide and Graphene Oxide-Mangane Oxide Nanocomposite

XPS was performed to detect the variations in the structure of the graphene oxide-mangane oxide nanocomposite during adsorption of the Se (VI) and Co(II). Fig. 6a shows extensively the XPS spectrum of the generated graphene oxide-mangane oxide nanocomposite. This figure shows the O 1s XPS spectra of mangane oxide-graphene oxide nanocomposite contained MnO_2. In this nanocomposite; Mn, O, and C elements are detected. The XPS spectra (Fig. 6b) shows two peaks located at 640.9 and 651.9 eV. This originated with the presence of Mn $2p_{3/2}$ and Mn $2p_{1/2}$ of Mn^{4+}. The maximum spectra exhibited similarities with the studies reported for MnO_2, indicating mangane is oxidated to Mn^{4+} [30]. The O 1s peak generated from two oxygenated groups. One of them is O^{2-} spectra of MnO_2 at a binding energy of 549.6 eV. The other one is an OH^- peak of manganese hydroxide. All these functional groups of graphene oxide were binded at a binding energy of 530.2 eV as reported by Pan et al., 2016 (Fig. 6c) [31]. The binding energy for Mn 2p of Graphene oxide M^2 increased during the adsorption of Se(VI) and Co(II) (Fig. 6c). This can be explained by to the formation of covalent Mn-O-Se or Mn-O-Co bonds by decreasing of extra-nuclear electron density around of the Mn as reported by Park et al., (2016) (data not shown) [30].

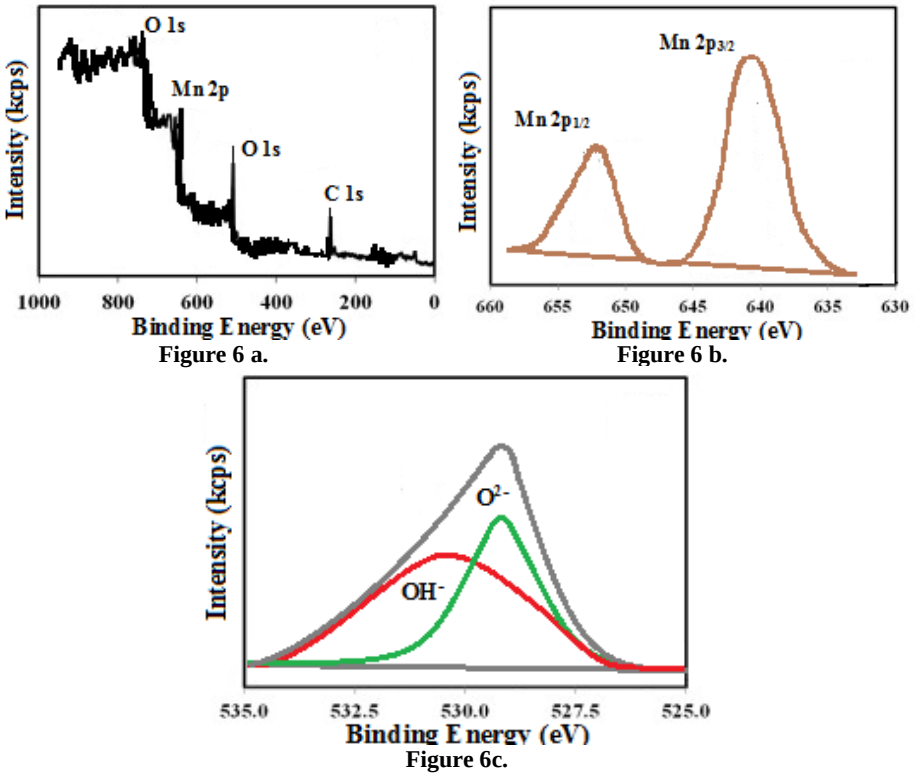

Figure 6. XPS spectra of a) narrow-scan O1s in graphene oxide-mangane oxide nanocomposite b) narrow-scan Mn 2p in graphene oxide-mangane oxide nanocomposite c) O^{2-} and OH^{-} peaks in graphene oxide-mangane oxide nanocomposite

3.8. Scanning Transmission Electron Microscopy (STEM) Analysis of Mangane Oxide, Graphene Oxide and GO-MnO Nanocomposite

In the STEM image, GO and MnO can be easily distinguished in Fig. 7a. It seems that the white is MnO only dispersed around the surface of GO (black particles). The small MnO nanocrystals dispersed around the GO-MnO nanoparticles form an oxide-on-oxide nanostructure. The grey ones are the GO-MnO Nanoparticles. As shown in Fig. 7b, the lattice spacing of a MnO nanocrystal was measured to be 1.47 nm, while the lattice spacing of the oxide nanocrystal adjacent to the GO nanoparticle was measured to be 1.49 nm, consisting to the (101) lattice plane of tetragonal spinel MnO (111). This image clearly shows the formation of the oxide-on-oxide nanostructures through close particle-on-particle contact between two oxides in this composite. As depicted from Fig. 7c, the formation of the special nanostructure may result from the epitaxial growth of MnO along the exposed (111) lattice plane of the GO. Since graphene oxide having a planer hexagonal structure, the spinel MnO can be rationalized to preferentially deposit on the surfaces of graphene through epitaxial growth of MnO as reported by Chou et al., (2014) [32].

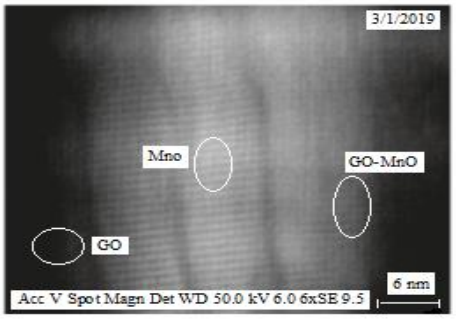

Figure 7a.

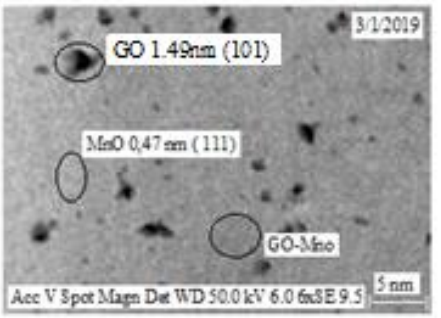

Figure 7b.

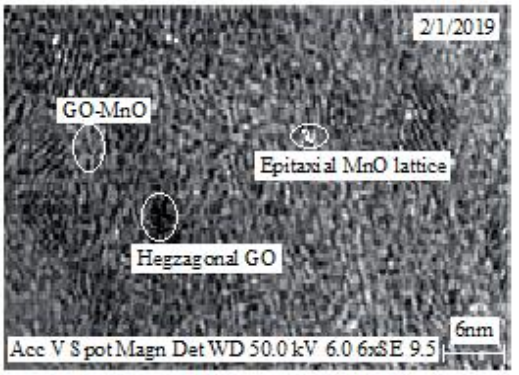

Figure 7c.

Figure 7. STEM picture of Mangane Oxide, Graphene Oxide and Mangane Oxide doped Graphene Oxide(a,b,c)

3.9. Termal Stability of Graphene Oxide, Mangane Oxide and Graphene Oxide-Mangane Oxide Nanocomposite- TGA analyss

Thermal stability of the graphene oxide-mangane oxide nanocomposite was investigated by TGA (Fig. 8). The samples showed three-step weight losses. Weight loss up to 98 °C temperature can be explained by the losses of water moieties bounded on the graphene oxide layers. Weight losses was detected at a temperature of 189 °C as reported by She et al., (2015) [33]. Lowering of the weight above 280 °C can be attributed to the thermal splitting of the carbon in the graphene oxide. Increasing of the thickness of the mangane oxide cause to the growth of the mass moieties (data not shown).This, is consistent with recent reports explaining that mangane oxide is thermally in equilibrium up to 1500 °C temperature [34].

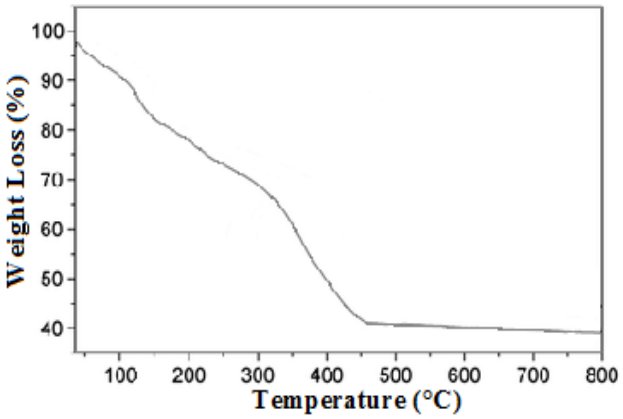

Figure 8. TGA lines of graphene oxide-mangane oxide nanocomposite

3.10. Effect of Increasing Graphene Oxide-Mangane Oxide Nanocomposite Concentrations on the Adsorption Yields of Se(VI) and Co(II)

The studies were performed at 2 mg/L graphene oxide-mangane oxide nanocomposite concentration since in the previous study the maximum adsorption yields of Se(VI) and Co(II) were obtained with this adsorbent concentration at a room temperature of 21 ^{o}C after 25 min (data not shown). As the graphene oxide-mangane oxide composite concentrations were elevated from 1 mg/L up to 4 mg/L the the adsorption yields of Se(VI) increased from 57% up to 98% (Table 3). Further increase of composite concentration to 5, 6 and 7 mg/L did not affect the Se(VI) adsorption yields. The adsorption yields remained maximum at a 4 mg/L graphene oxide-mangane oxide composite at 21 ^{o}C. Similar results was found for Co(II). The maximum adsorption yields for Co (II) was obtained at 4 mg/L graphene oxide-mangane oxide composite concentration (Table 3). Increasing of the composite concentration did not affect the adsorption yield of Co(II). These results showed that the adsorption yields of both metals depend to the nanocomposite concentration up to 5 mg/L. This can be explained with elevated ion exchange capability of the graphene oxide-mangane oxide nanocomposite. The results showed that Co(II) and Se(VI) adsoption yields increases up to an optimum concentration in which the removal yield has no change with the graphene oxide-mangane oxide composite concentration as reported by Somiya et al., (1988) and Matias et al., (2015) [35], [36]. As known, the equilibrium concentration of graphene oxide-mangane oxide nanocomposite lowered with elevating nanocomposite concentrations. At high nanocomposite concentration the unit adsorption decrease due to adsorption sites remaining unsaturated during the adsorption reaction whereas the number of sites available for adsorption site increases by increasing the adsorbent dose as reported by Somiya et al., (1988) and Matias et al., (2015) [35], [36].

Table 3. Effects of increasing graphene oxide-mangane oxide nanocomposite concentrations on the adsorption yields of Se(VI) and Co(II) levels at 21 ^{o}C after 25 min at increasing graphene oxide-mangane oxide composite concentration

Graphene oxide-mangane oxide Concentration (mg/L)	Se(VI) Concentration (mg/ L)	Se(VI) removal Efficiency (%)	Co (II) Concentration (mg/ L)	Co(II) removal efficiency (%)
1	2,5	57	2,5	55
2	2,5	64	2,5	63
3	2,5	77	2,5	75
4	2,5	98	2,5	98
5	2,5	98	2,5	98
6	2,5	98	2,5	98
7	2,5	98	2,5	98

A multiple linear relationship between maximum adsorption yields of Se(VI) and Co(II) and graphene oxide-mangane oxid nanocomposite concentrations up to 5 mg/L graphene oxide-mangane oxide nanocomposite was obtained (R=0.93) and this regression was significant (ANOVA $p=0.005<\alpha$ (0.05) and F=1.28). Further increase of graphene oxide-mangane oxide nanocomposite concentration did not affect both Co(II) and Se(VI) adsorptions.

3.11. Effects of Contact Time on the Adsorption Capacities of Co(II) and Se(VI)

The studies were performed at 4 mg/L graphene oxide-mangane oxide composite concentration to determine the effects of adsorption time on the adsorption yields of Se(VI) and Co(II) at 21 ^{o}C. Table 4 shows the effect of contact time on the adsorption capacities of Se(VI) and Co(II) by 4 mg/ L graphene oxide-mangane oxide nanocomposite.

Table 4. Effects of contacting time on the adsorption capacities of Co(II) and Se(VI) at 4 mg/ L graphene oxide-mangane oxide nanocomposite at 21 ^{o}C

Graphene Oxide-Mangane Oxide Concentration (mg/L)	Contacting Time for Adsorption (min)	Se(VI) Concentration (mg/ L)	Se(VI) Removal efficiency (%)	Se(VI) adsorption capacity (mg/g)	Co(II) Concentration (mg/ L)	Co(II) Removal efficiency (%)	Co(II) adsorption capacity (mg/g)
4	20	2.5	98	289	2.5	98	256
4	30	2.5	95	270	2.5	90	248
4	50	2.5	90	259	2.5	89	230
4	60	2.5	86	239	2.5	80	190
4	70	2.5	69	200	2.5	60	160
4	80	2.5	54	160	2.5	43	145

The adsorption capacity of nanocomposite increases with time and attain equilibrium within 20 min for both metals. The equilibrium time was dependent up to 30 min adsorption. Then, the increase of contacting time did not affect the adsorption capacities of both metals. It was found that Se(VI) adsorption capacity (289 mg/g) was higher than Co(II) adsorption capacity (256 mg/g) after 20 min adsorption/contacting time at 4 mg/L nano graphene oxide-mangane oxide nanocomposite. The metal absorption versus time are simultaneously elevated the saturation

gradient. This can be explained by the possible monolayer bounding of metal ions on the surrounding of the adsorbent up to a contacting time of 20 min. Later, the lower adsorption rate at high contact times is due to a decrease in number of vacant sites of nanocomposite and metal concentrations. The decreased adsorption rate, particularly, toward at high contact times, indicates the possible monolayer formation of metals on the adsorbent surface. This may be attributed to the lack of available active sites required for further uptake after attaining the equilibrium.

A multiple linear relationship between maximum adsorption yields of Se(VI) and Co(II) and adsorption times up to 30 min was obtained (R=0.93) and this regression was significant (ANOVA $p=0.003<\alpha$ (0.05) and F=1.06). Further increase of contacting time did not affect both Co(II) and Se(VI) adsorption yields.

3.12. Effect of pH on the Adsorption Yields of Co(II) and Se(VI)

The effect of pH on the Co(II) and Se(VI) adsorption at 4 mg/L graphene oxide-mangane oxide nanocomposite at 21^{o}C at 20 min contacting time for pHs between 2.2 and 10.0 is presented in Table 5. It can be found that the adsorption yields increased with pH for both metals. The uptake of Co(II) and Se(VI) by graphene oxide-mangane oxide nanocomposite increased as the pH increased from 2.0 to 6.1. At higher pH values (8.0-8.9) the adsorption efficiency increased for both metals. As the pH of the samples elevated to >9.3; Co(II) started to accumulated in the solution. Therefore, the elevated mass of adsorption at pH = 8.9 may be a synergistic effect of both adsorption and accumulation on the monolayer surrounding of the graphene oxide-mangane oxide nanocomposite. It is considered that graphene oxide-mangane oxide had a maximum adsorption capacity at a pH of 8.9. Therefore, the optimum pH for maximum Co(II) and Se(VI) adsorption is 8.9. Similarly, Se(VI) adsorption on the graphene oxide-mangane oxide composite tends to elevate with the increasing of pH. This can be explained by the positively charges occured at low pHs. Therefore, the adsorption of Se(VI) at lower pH values resulted from an increased repulsion between the more positively charged Se species and positively charged surface sites. Furthermore, at lower pH, H^+ ions were competitive with Se(VI) ions to binding on the surface of the nanocomposite [37]. The adsorption efficiencies of Se(VI) and Co(II) increased from 43% to 87% and up to 98% as the pH were increased from 2 to 4 and up to 8.9. In our study adsorption efficiency was directly dependent to the pH. For the graphene oxide-mangane oxide nanocomposite, the adsorption at pH above 9.5 shows a reduction due to the formation of hydroxylic functional groups of cobalt and selenium such as $Co(OH)_2$) and ($Se(OH)_2$) [38].

Table 5. Effect of pH on the adsorption efficiency of Se(VI) and Co(II) at 4 mg/L graphene oxide-mangane oxide nanocomposite after 20 min adsorption time

Graphene Oxide-Mangane Oxide Concentration (mg/L)	pH	Se(VI) Concentration (mg/ L)	Se(VI) Removal efficiency (%)	Se(VI) adsorption capacity **(**mg/g**)**	Co(II) Concentration (mg/ L)	Co(II) Removal efficiency (%)	Co(II) adsorption capacity **(**mg/g**)**
4	2.2	2.5	56	289	2.5	53	256
4	4.5	2.5	69	270	2.5	67	248
4	6.2	2.5	72	259	2.5	70	230
4	8.9	2.5	98	239	2.5	98	190
4	10.0	2.5	87	200	2.5	80	160

3.13. Adsorption Properties and Kinetics of Se(VI) and Co(II) with Constant Graphene Oxide-Mangane Oxide Nanocomposite

The adsorption of Se(VI) and Co(II) onto 4 mg/L graphene oxide-mangane oxide nanocomposite reached equilibrium within 20 min at 21 ^{o}C at pH=8.9. The adsoption kinetic data for both 1.5 mg/L Se(VI) and Co(II) were described by the pseudo-first order kinetic models for graphene oxide-mangane oxide, respectively (Fig. 9). The Se(VI) and Co(II) adsorption on the surface of graphene oxide-mangane oxide before reach to equilibrium can be explained by two steps: at the beginning an initial quik phase (0–4 min) followed by a slow phase (4–6 min). The low phase was originated from the pore diffusion within graphene oxide-mangane oxide as reported by Wan et al., (2018) [39].

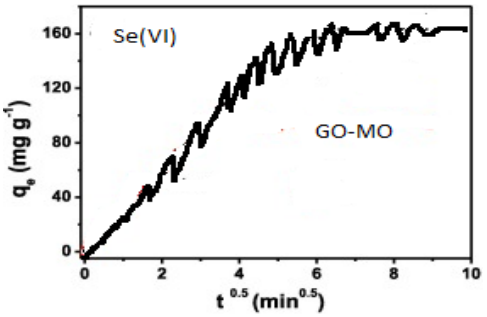

Figure 9a. Adsorption kinetic of 1.5 mg/L Se(VI) (a) onto 4 mg/L

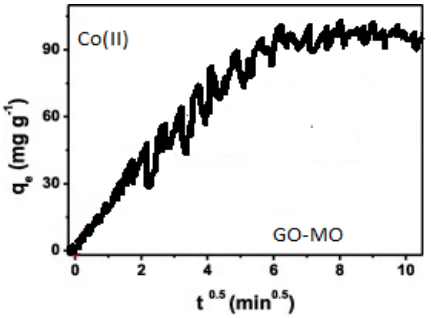

Figure 9b. Adsorption kinetics of 1.5 mg/L Co(II) (b) onto 4 mg/L

Figure 9. Adsorption kinetics of 1.5 mg/L Se(VI) (a) and 1.5 mg/L Co(II) (b) onto 4 mg/L graphene oxide-mangane oxide at pH = 8, 9, and at a temperature of 21 ^{o}C.

3.14. Recoveries of Se(VI) and Co(II)

The adsorption efficiencies in both metals were not reduced significantly after four sequential utilization of 4 mg/L graphene oxide-mangane oxid nanocomposite within 20 min contacting time (Table 6). In this research, the adsorption yields of Se(VI) and Co(II) were 99% and 98% in the first utilization. After four sequential utilization of the same graphene oxide-mangane oxide nanocomposite the adsorption yields of Se(VI) and Co(II) decreased slightly from 90 and to 86 %, respectively.

Table 6. Sequential treatment of Se(VI) and Co(II) with 4 mg/L graphene oxide-mangane oxide nanocomposite concentration, after 20 min adsorption time at pH 8.9 and at a temperature of 21^{o}C.

	Sequential cycles			
	First	Second	Third	Fourth
For Se(VI)	99	97	95	90
For Co(II)	98	93	90	86

4. COST ANALYSIS

A cost analysis was carried out for the adsorption of Se(VI) and Co(II) from 1 m^3 simulated glass and metal industry wastewaters at optimum experimental conditions. The total cost of the

adsorptions of Se(VI) and Co(II) from 1 m^3 glass and metal industry wastewaters were found as 0.41 € and 0.51 €, respectively, at the optimum experimental conditions with graphene oxide-mangane oxid nanocomposite (Table 7). 0.08 € was spent for electricity costs for glass and metal industries for adsorptions of Se(VI) and Co(II), while the chemical cost of synthesizing the graphene oxide-mangane oxid nanocomposite for Se(VI) was 0.12 € while the chemical cost was 0.22 € for Co(II) (Table 7). The apparatus cost used during the syhnthesis of graphene oxide-mangane oxid nanocomposite was 0.21 €. In this study, the main part of the cost consisted of the chemicals using in the preparation of graphene oxide-mangane oxide nanocomposite. The cost is mainly consisted from the chemicals used in preparation of nanocomposite Since this nanocomposite was produced under laboratory conditions can be used four times for adsorptions of Se(VI) and Co(II) with yields as high as 90% and 86%. This reduce the adsorption costs to from 0,41€ and 0,51€ to 0.21 € and 0.29 € for Se(VI) and Co(II), respectively.The total adsorption cost reduced by 48% and 43% for Se(VI) and Co(II) respectively.

Table 7. Cost analysis for the treatment of Se(VI) and Co(II) with graphene oxide-mangane oxid adsorption

Cost Analysis	Treatment of glass and metal industry wastewaters with graphene oxide-mangane oxide
Electricity consumption	Electricity cost for rapid stirring in a mixer for 20 min= 0.02 €, Electricity cost for an oven at 298 K =0.04 €, Electricity cost for incubation at an incubator =0.02 €.
Chemicals	For preparation of graphene oxide-mangane oxide nanocomposite: 1. 15 g graphite powder = 0.04 € , 2. 15 g graphene oxide standard = 0.02 €. 3. 15 g mangane oxide standard = 0.03 €, 4. 0.1 M Mn SO_4 = 0.03€ 5. 14 g Mn(II) = 0.02 € 6. 1 M NaOCl = 0.02 € 7. 1 M NaOH = 0.02 € 8. 1mM HCl = 0.01€ 9. 1mL Se standard = 0.01 € 10. 1 mL Co standard = 0.01€ 12. 5 mL H_2O_2 = 0.01€
Apparatus	Shaker for half hour utilization = 0.06 € Incubator for half hour utilization = 0.09 € Centrifuge for half hour utilization = 0.03 € Sonicator for half hour utilization = 0.03 €
Total cost for treatment of Se(VI) from 1m^3 glass industry wastewater	0.41€
Total cost for treatment of Co(II) from 1m^3 metal industry wastewater	0.51€

5. CONCLUSIONS

The results of this study showed that Se(VI) and Co(II) from glass and raw metal industry wastewaters can be effectively removed with adsorption process using the nanocomposite namely

graphene oxide-mangane oxide prepared under laboratory conditions. SEM analysis showed that graphene oxide has a smooth surface while mangane oxide was detected in the upper layer of the graphene oxide-mangane oxide nanocomposite. EDS analysis showed that graphene oxide has the smallest surface area (32 m^2/g) and pore volume (0.11 cm^3/g) compared to mangane oxide. HR-TEM studies showed that graphene oxide-mangane oxide nanocomposite exhibited a crystal structure. The XPS spectra showed two peaks located at 640.9 and 651.9 eV originating from the Mn $2p_{3/2}$ and Mn $2p_{1/2.}$ The STEM analysis exhibited that that majority of the doped Au atoms are dispersed entirely in the $MnO_{2.}$ The nanocomposite showed three-step weight losses: Weight loss up to 98 °C temperature could be attributed to the dehydration of water molecules absorbed on the graphene oxide surface. Weight losses were observed at a temperature of 189 °C. Lowering of the weight above 280 °C resulting due to the thermal degradation of carbon in the graphene oxide. For maximum Se(VI) (98%) and Co(II) yields (98%) the optimum operational conditions were as follows: graphene oxide-mangane oxide nanocomposite concentration, pH and adsorption time were 4 mg/L, 8.9 and 20 min, respectively, at a room temperature of 21^oC. It was found that Se(VI) was adsorbed with high yields (289 mg/g) compared Co(II) (256 mg/g). Pseudo-first order model explained the adsorption kinetic of Se(VI) and Co(II) onto graphene oxide-mangane oxide nanocomposite. The same graphene oxide-mangane oxide nanocomposite can be sequentially utilized for four times with yields as high as 90% and 86% for Se(VI) and Co(II), respectively. Therefore, the adsorption costs reduced from 0.51 € (for Co(II)) and from 0.41 € (for Se(VI)) to 0.29 € and to 0.21 €, respectively, with cost reduction yields of 43% and 48%.

REFERENCES

[1] Lawson S., Macy J.M., (1995) Bioremediation of selenite inoil refinerywastewater, *Appl.Microbiol. Biotechnol.* 43 (4) 762–765.

[2] Peak D., (2006) Adsorption mechanisms of selenium oxyanions at the aluminum oxide/water interface, *J. Colloid Interface Sci.* 303 337–345.

[3] Das J., Das D., Dash G.P., Parida K.M., (2002) Studies on Mg/Fe hydrotalcite-likecompound (HTlc). I. Removal of inorganic selenite (SeO32−) from aqueous medium, *J. Colloid Interface Sci*. 251 (1) 26–32.

[4] Duc M., Lefèvre G., Fédoroff M., (2006) Sorption of selenite ions on hematite, *J. Colloid Interface Sci.* 298 (2) 556–563.

[5] Afkhami A., (2002) Kinetic-spectrophotometric determination of selenium in natural water after preconcentration of elemental selenium on activated carbon, *Talanta* 58, 311–317.

[6] El-Shafey E.I., (2007) Removal of Se(IV) from aqueous solution using sulphuric acidtreated peanut shell, *J. Environ. Manage*. 84, 620–627.

[7] Martínez M., Giménez J., Pablo J., Rovira M., Duro L., (2006) Sorption of selenium (IV) and selenium (VI) ontomagnetite, *Appl. Surf. Sci.* 252 (10) 3767–3773.

[8] Wan S., Wu J., He F., Zhou S., Wang R., Gao B., Chen J ., (2017) Hosphate removal by leadexhausted bioadsorbents simultaneously achieving lead stabilization, *Chemosphere* 168, 748–755.

[9] Wan S, Ding W, Wu J, Gu Y, He F., (2018) Manganese oxide nanoparticles impregnated graphene oxide aggregates for cadmium and copper remediation, *Chemical Engineering Journal*, 350, 1135-114.

[10] Swann S.Jr., Appel E.G., Kistler S.S., (1934) Thoria aerogel catalyst: aliphatic esters to ketones Ind, *Eng. Chem.* 26, 1014–1014.

[11] Adebajo M., Frost R., Kloprogge J., Carmody O., Kokot S., (2003) Porous materials for oil spill cleanup: a review of synthesis and absorbing properties, *J. Porous Mater.* 10 159–170.

[12] Long J.W., Fischer A.E., McEvoy T.M., Bourg M.E., Lytle J.C., Rolison D., (2008) Selflimiting electropolymerization en route to ultrathin, conformal polymer coatings for energy storage applications, *PMSE Prepr*. 99 772–773.

[13] Latthe S.S., Digambar Y.N., Rao A.V., (2009) TMOS based water repellent silica thin films by co-precursor method using TMES as a hydrophobic agent, *Appl. Surf. Sci*. 255 3600–3604.

[14] Fan H., Anderson P., (2005) Copper and cadmium removal by Mn oxide-coated granular activated carbon, *Sep. Purif. Technol.* 45, 61–67.

[15] Boujelben J.B.N., Elouear Z., (2009) Removal of lead (II) Ions from aqueous solutions using manganese oxide-coated adsorbents: characterization and kinetic study, *Adsorpt. Sci. Technol.* 27, 177–191.

[16] Wang L., Han C., Nadagouda M.N., Dionysiou D.D., (2016) An innovative zinc oxide-coated zeolite adsorbent for removal of humic acid, *J. Hazard. Mater*. 313, 283–290.

[17] Ali I., (2012) New generation adsorbents for water treatment, *Chem. Rev.* 112, 5073–5091.

[18] Zhang Q., Du Q., Hua M., Jiao T., Gao F., Pan B., (2013) Sorption enhancement of lead ions from water by surface charged polystyrene-supported nano-zirconium oxide composites, *Environ. Sci. Technol*. 47, 6536–6544.

[19] Liu Z., Robinson J.T., Sun X., Dai H., (2008) PEGylated nanographene oxide for delivery of water-insoluble cancer drugs, *J. Am. Chem. Soc* 130, 10876–10877.

[20] Shen Y., Chen B., (2015) Sulfonated graphene nanosheets as a superb adsorbent for various environmental pollutants in water, *Environ. Sci. Technol.* 49, 7364–7372.

[21] Sun Y., Tang J ., Zhang K ., Yuan J ., Li J ., Zhu D.M., Ozawa K., Qin L.C., (2017) Comparison of reduction products from graphite oxide and graphene oxide for anode applications in lithium-ion batteries and sodium-ion batteries, *Nanoscale* 9, 2585–2595.

[22] Whitby R.L.D., Gun'ko V.M., Korobeinyk A., Busquets R., Cundy AB., Laíszlo K., Skubiszewska-Zie J., Kovacs K., Mikhalovsky S.V., (2012) Driving forces of conformational changes in single-layer graphene oxide, *ACS Nano* 5, 3967–3973.

[23] Wan S., Qu N., He F., Wang M., Liu G., He H., (2015) Tea waste-supported hydrated manganese dioxide (HMO) for enhanced removal of typical toxic metal ions from water, *RSC Adv*. 5, 88900–88907.

[24] Wan W., Zhao Z., Timothy C.H., Qian B., Peng S., Hao X., Qiu J., (2015) Graphene oxide liquid crystal Pickering emulsions and their assemblies, *Carbon* 85 16–23.

[25] Jamali M.R., Soleimani B., Rahnama R., Rahimi S.H.A., (2012) Development of an in situ solvent formation microextraction and preconcentration method based on ionic liquids for the determination of trace cobalt (II) in water samples by flame atomic absorption spectrometry, http://dx.doi.org/10.1016/j.arabjc.2012.08.004.

[26] Ma J., Liu C., Li R., Wang J., (2012) Properties and structural characterization of oxide starch/chitosan/graphene oxide biodegradable nanocomposites, *J. Appl. Polym. Sci*. 123, 2933–2944.

[27] Li Y., Du Q., Liu T., Peng X., Wang J., Sun J., Wang Y., Wu S., Wang Z., Xia Y., Xia L., (2013) Comparative study of methylene blue dye adsorption onto activated carbon, graphene oxide, and carbon nanotubes, *Chemical Engineering Research and Design*, 91, 2, 361-368, https://doi.org/10.1016/j.cherd.2012.07.007.

[28] Amir F.Z., Pham V.H., Schultheis E.M., Dickerson J.H., (2018) Flexible, all-solid-state, high-cell potential supercapacitors based on holey reduced graphene oxide/manganese dioxide nanosheets, *Electrochimica Acta*, 260, 944-951, https://doi.org/10.1016/j.electacta.2017.12.071.

[29] Jasinski J.B., Ziolkowska D., Michalska M., Kaminska M., (2013)Novel graphene oxide/manganese oxide Nanocomposites, RSC Advances 3(45):22857-22862, DOI:10.1039/C3RA42254B.

[30] Park S. K. , Hoon D., Ho S., Park S., (2016) Electrochemical assembly of reduced graphene oxide/manganese dioxide nanocomposites into hierarchical sea urchin-like structures for supercapacitive electrodes, *Journal of Alloys and Compounds*, 668, 146-151,https://doi.org/10.1016/j.jallcom.2016.01.214.

[31] Pan N, Li L, Ding J, Li S., Wang R., Jin Y., Wang X., Xia., (2016) Preparation of graphene oxide-manganese dioxide for highly efficient adsorption and separation of Th(IV)/U(VI), *Journal of Hazardous Materials* 309, 107-115, https://doi.org/10.1016/j.jhazmat.2016.02.012.

[32] Chou T., Doong R., Hu C. C., Zhang B., Su D.S., (2014) Hierarchically Porous Carbon with Manganese Oxides as Highly Efficient Electrode for Asymmetric Supercapacitors, *ChemSusChem*, 7, 3, https://doi.org/10.1002/cssc.201301014.

[33] She X., Zhang X., Liu J., Li L., Yu X., Huang Z., Shang S., (2015) Microwave-assisted synthesis of Mn_3O_4 nanoparticles@reduced graphene oxide nanocomposites for high performance supercapacitors, *Materials Research Bulletin*, 70, 945-950, https://doi.org/10.1016/j.materresbull.2015.06.044.

[34] Qu J., Gao F., Zhou Q., Wang Z., Hu H., Li B., Wan W., Wang X., Qiu J., (2013) Highly atom-economic synthesis of graphene/Mn_3O_4 hybrid composites for electrochemical supercapacitors, *Nanoscale*, 5, 7, 2999-3005.

[35] Somiya S., Yamamato N., Yanagina H., (1988)Science and Technology of Zirconia (III), 24A and 24B, *American Ceramic Society*, Westerville.

[36] Matias T., Marques J., Quina M.J., Gando-Ferreira L., Valente A.J.M., Portugal A., Durães L., (2015) Silica-based aerogels as adsorbents for phenol-derivative compounds, *Colloids Surf. A* 480, 260–269.

[37] Caiping Y., (2010) Adsorption and desorption properties of D151 resin for Ce(III), *Journal of rare earths*, 28, Spec. Issue, Dec. p. 183 DOI: 10.1016/S1002-0721(10)60324-9.

[38] Jiang L., Liu Y., Zeng G., Xiao F., Hu X., Hu X., Wang H., Li T., Zhou L., Tan X., (2016) Removal of 17β-estradiol by few-layered graphene oxide nanosheets from aqueous solutions: External influence and adsorption mechanism, Xiao-fei, *Chem. Eng. J.* 284 93–102, http://doi.org/10.1016/j.cej.2015.08.139.

[39] Wan S., Wu J., Zhou S., Wang R., Gao B., He F. (2018) Enhanced lead and cadmium removal using biochar-supported hydrated manganese oxide (HMO) nanoparticles: Behavior and mechanism, *Sci. Total Environ.* 616–617, 1298–1306.